In situ TEM study of fractal formation in amorphous Ge/Au bilayer films

Shuyuan Zhang*
Structure Research Laboratory, University of Science and Technology of China, Hefei 230026, China

Xiaoping Wang
Fundament Physics Center, University of Science and Technology of China, Heifei 230026, China

Zhiwen Chen
Structure Research Laboratory, University of Science and Technology of China, Hefei 230026, China

Ziqin Wu
Fundament Physics Center, University of Science and Technology of China, Hefei 230026, China

N. Y. Jin-Phillipp, M. Kelsch, and F. Phillipp
Max-Planck-Institut fur Metallforschung, Heisenbergstrasse 1, D-70569 Stuttgart, Germany
(Received 11 December 1998)

The kinetic behavior of fractal crystallization in amorphous semiconductor/metal bilayer films has been studied by *in situ* transmission electron microscopy. The fractal growth process exhibits three stages: rapid growth, steady growth, and slow growth. During the initial rapid growth stage, the fractal crystallization is controlled by both diffusion and reaction processes. With increasing annealing time, fractal growth is obstructed and becomes slower because more and more other fractal patterns approach from the neighborhood. The growth kinetics analysis indicates that both diffusion-limited aggregation and random successive nucleation mechanisms play an important role in fractal crystallization in the amorphous Ge/Au films. [S0163-1829(99)05031-6]

INTRODUCTION

In amorphous semiconductor/metal (a-S/M) bilayer or multilayer systems, the crystallization of amorphous semiconductors has attracted much attention because the metal can dramatically reduce the crystallization temperature of the amorphous semiconductor.[1–5] Such behavior is sometime called ''metal-induced crystallization (MIC)''[2] or ''metal-mediated crystallization (MMC).''[6] During the MIC or MMC process, complex morphologies of semiconductor crystallites appear in the films, and can be characterized as fractal patterns. The formation of the fractal morphology is closely related to the mechanism of the crystallization of the semiconductor. In recent years the fractal crystallization behavior in metal/amorphous semiconductor bilayer films has been widely studies.[7–17] Leriah *et al.* observed the dense branching morphology of Ge crystallites in annealed Ge-Al amorphous films, and the growth morphology was explained on the basis of the diffusion-limited aggregation (DLA) model[9,10] and the modified DLA model.[11,12] Sugawara *et al.*[13] studied the growth dynamics of a Ge fractal in a-Ge/Au bilayers and suggested that the growth was diffusion-controlled by Ge atoms in a Ge-depleted zone surrounding a Ge cluster. The fractal morphology was explained in terms of the diffusion length and the size of the Au crystallites. Based on their experimental results of the annealing behavior of a-Ge/Au bilayers, Hou and Wu[7] proposed a ''random successive nucleation (RSN)'' model. Li *et al.*[8] and Petford-Long *et al.*[18] supported the RSN mechanism of fractal crystallization by investigating an Al/a-Ge bilayer system. Recently Bian *et al.*[14,15] investigated the fractal formation in a-Ge/Au bilayer films by *in situ* plane-view and cross-section TEM observations. They considered that the DLA model might not be suitable to describe fractal growth in a-Ge/p-Au (polycrystalline Au) films and supported the random successive nucleation and growth (RSNG) mechanism to explain their results.

Up to now there has been no generally accepted understanding for the microscopic mechanism of fractal formation in metal/amorphous semiconductor bilayer films. More insight into this phenomenon is needed. Recent studies suggested that fractal crystallization is closely related to the growth kinetics,[18,19] which involves the fractal crystallization area (S) and the annealing time (t). In order to obtain a quantitative relationship between S and t, *in situ* TEM observationis helpful and necessary because it can record the complete sequence of events continuously and determine the growth kinetics precisely. In this paper, quantitative *in situ* TEM studies of fractal crystallization kinetics in Au/a-Ge bilayer films are reported.

EXPERIMENT

Ge and Au were sequentially deposited onto Si(100) substrates (by an evaporator) in vacuum of about 2×10^{-5} torr with the substrate at room temperature. Samples with two thickness ratios were prepared as follows:

Sample	1	2
Au (nm)/a-Ge (nm)	30/30	35/25

After evaporation, the samples were cut into small circular wafers with a radius of 1.5 mm by the ultrasonic disk

 ©1999 The American Physical Society

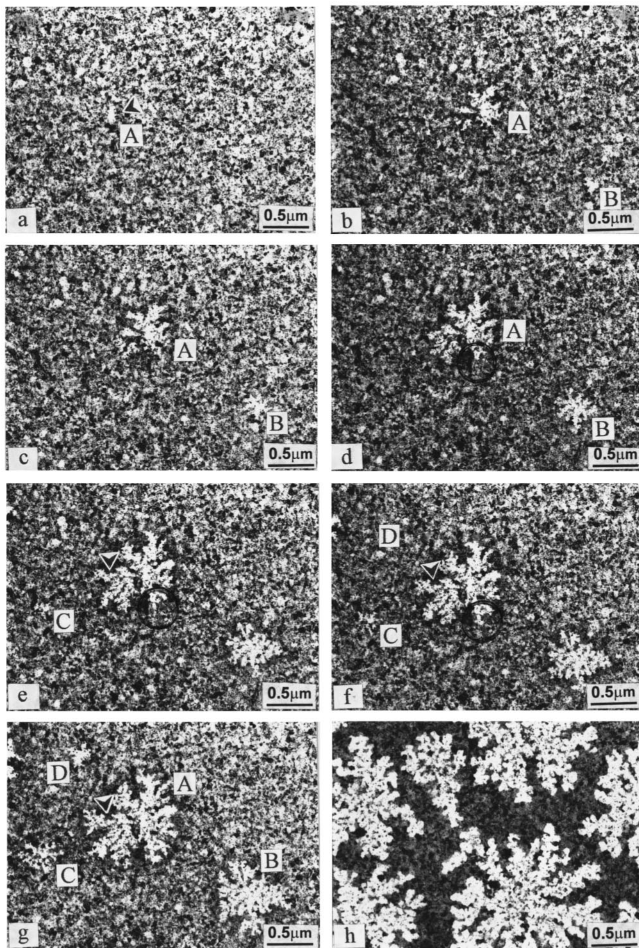

FIG. 1. Fractal crystallization process in sample 1 (a) 110 °C, 10 min+120 °C, 5 min; (b) 120 °C, 15 min; (c) 120 °C, 25 min; (d) 120 °C, 33 min; (e) 120 °C, 40 min; (f) 120 °C, 45 min; (g) 120 °C, 55 min; (h) 120 °C, 55 min+135 °C, 10 min.

cutter. Then the wafers were polished to about 30 μm thickness with the disk grinder. The dimple grinder was used to thin the wafer thickness less than 5 μm. Finally the wafers were milled by the ion polishing system. During the processes mentioned above only the sides of the Si substrates were polished, dimpled, and milled, thus Au/a-Ge bilayers remained. TEM *in situ* observations were carried out on a JEOL 4000 FX transmission electron microscope equipped with a heating stage. During heating, fractal crystallization occurred in the two samples, and the processes of the fractal crystallization were recorded. TEM photographs with fractal patterns were digitized by a scanner with a resolution of 200 DPI. Using a fractal image process software (FIPS) developed by Wang,[20] the fractal patterns may be processed. Many parameters, such as fractal dimension size and radius of gyration of each fractal pattern, were obtained. The fractal dimensions were calculated by the box-counting method.

RESULTS

In situ observation of fractal growth process

Figures 1(a)–1(h) show the fractal growth process in sample 1. It can be seen from Fig. 1 that three different

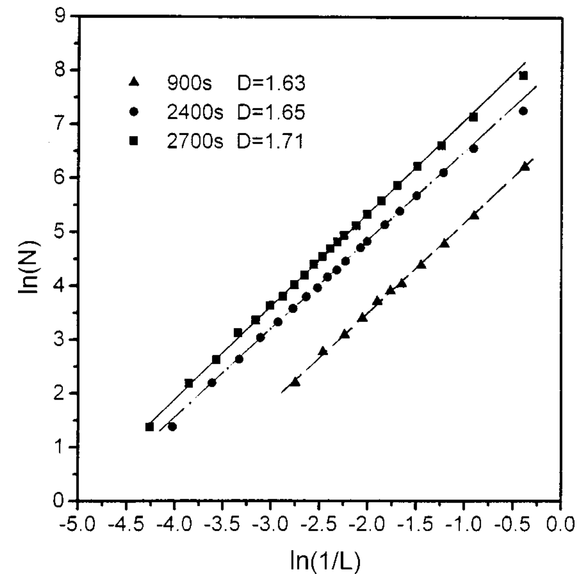

FIG. 2. The plots of $\ln N$ vs $\ln 1/L$ of the snowflakelike p-Ge regions (marked A) in Figs. 1(c), 1(e), and 1(g), respectively, where L is the box size and N represents for the number of boxes occupied by the Ge crystallites. The plots have good linearity.

contrasts (dark, dark gray, and white) exist in all micrographs. Since the electron scattering of Au is much stronger than that of Ge, the dark contrast is mainly from Au grains, the white contrast is from Ge clusters, and the dark gray contrast comes from the mixed regions of Au and Ge. At temperature below 110 °C, no significant structure change occurred. When temperature reached 110 °C for 10 min and then 120 °C for 5 min, the crystallization of amorphous Ge (a-Ge) started, as shown by an arrow in Fig. 1(a). The crystalline Ge (c-Ge) cluster, labeled A, gradually showed the snowflakelike fractal morphology after 20 min at 120 °C. During further annealing up to 55 min at the same 120 °C. [Figs. 1(c)–1(g)], the branches of the snowflakelike morphology continuously extended and some new patterns appeared one after another at other sites in the film, as labeled with B, C, and D. When the temperature was raised to 135 °C, the polycrystalline Ge (p-Ge) morphologies dramatically covered the whole area of the film. Figure 2 shows three plots of $\ln N$ versus $\ln(1/L)$ of the snowflakelike p-Ge regions in Figs. 1(c), 1(e), and 1(g), respectively, where L is the box size (the maximum values of the three p-Ge regions are 600, 850, and 1050 nm, respectively) and N represents for the number of boxes occupied by the Ge crystallites. It can be seen that the three plots have good linearity, which means that the snowflakelike morphologies have the scale invariance in these ranges. So the snowflakelike Ge patterns can be regarded as fractals. The fractal crystallization process exhibits the following characteristics. (i) As long as the nucleation of a-Ge started at one site, a-Ge around this site crystallized quite fast, which indicated that latent heat released due to crystallization of a-Ge played an important role in fractal formation. (ii) The tips of fractal branches always contacted directly with the dark gray contrast regions during heating as shown by the circles from Figs. 1(d)–1(f), and the fractal branches extended along the dark gray regions in general. (iii) The tip directly contacted with the dark re-

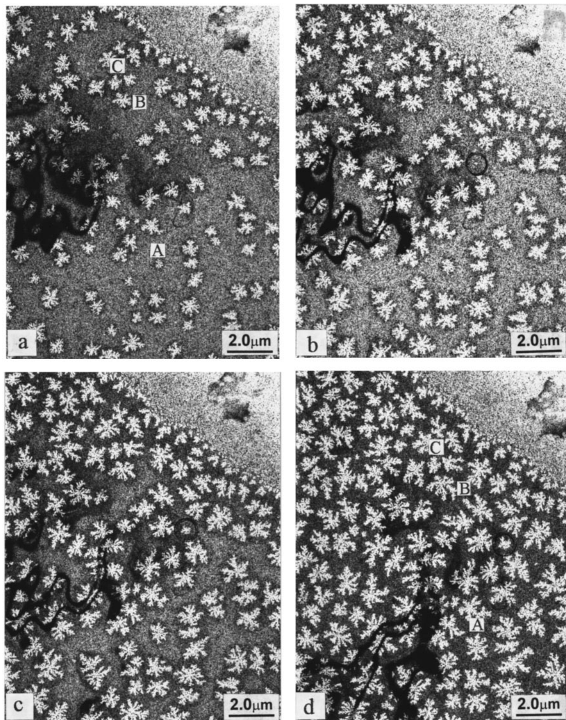

FIG. 3. Fractal crystallization process in sample 2 (a) 130 °C, 5 min; (b) 130 °C, 7.5 min; (c) 130 °C, 10 min; (d) 130 °C, 20 min.

gion, as marked by an arrow in Figs. 1(e)–1(g), hardly advanced, implying that Au grains reduced the diffusion of Ge into the fractal region.

The fractal crystallization process in sample (ii) is shown in Figs. 3(a)–3(d) at much lower magnification. The nucleation took place very rapidly in this case, and most fractals nucleated already in 5 min at 130 °C. The size of the fractal patterns increased gradually and a few new fractal patterns formed (as shown by the circles) with increasing heating time.

$S \sim t$ relationship

The fractal patterns obtained in the *in situ* observation were processed by computer. Figure 4 shows the $S \sim t$ curves of four fractal patterns, A–D, in Fig. 1 during 120 °C annealing. The intersection points t_0 of B, C, and D curves with the abscissa, in fact, represent the incubation time of B, C, and D fractal patterns, respectively. It can be seen that the curves are nonlinear, which indicates that the relationship between S and $(t-t_0)$ obeys a power law with an index larger than 1. Figure 5 exhibits the $S \sim t$ curves of three fractal pattern A, B, and C at 130 °C heating in Fig. 3. It should be noted that the conditions around the A, B, and C fractal patterns are different after heating for 5 min at 130 °C, as shown in Fig. 3(a). Fractal A can be called an easily developed pattern since it is far away from the other patterns. Fractals B and C are partially obstructed and obstructed patterns, respectively, because some other patterns are close to B and many to C. The $S \sim t$ curves of fractal patterns of different types exhibit different characteristics. The curve for fractal A shows "∫" shape, but the curves for fractals B and C look like the latter part of that for fractal A. This interesting result will be discussed later.

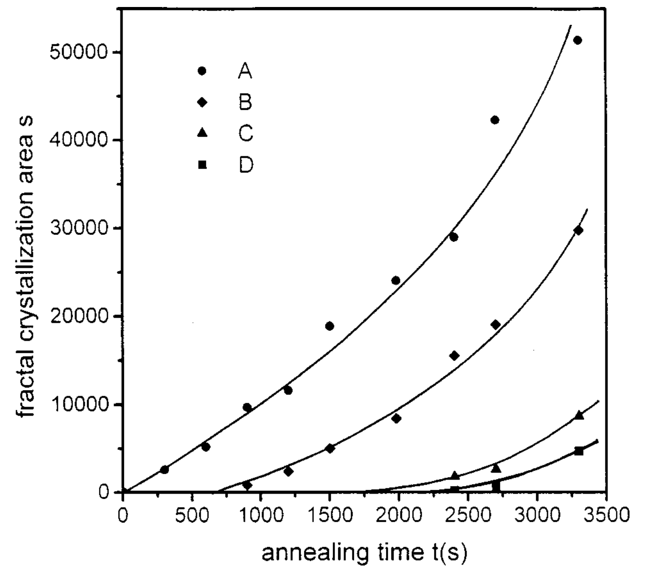

FIG. 4. $S \sim t$ curves of four fractal patterns A, B, C, and D in Fig. 1 during 120 °C annealing.

$R_g \sim t$ relationship

From the same fractal images, the radii of gyration of fractal patterns can be obtained. Figure 6 shows the relationship between R_g and annealing time t for the fractal patterns A, B, C, and D in Fig. 1. It is evident that $R_g \sim (t-t_0)$ curves also obey a power law. However, the increasing rates of R_g for various fractal patterns are different.

Fractal dimensions

The fractal dimensions of patterns during the various stages of fractal crystallization have been calculated by the box-counting method. Figure 7 shows the development of fractal dimensions of patterns A, B, and C in Fig. 1. It is evident that the fractal dimension increases in general with increasing annealing time.

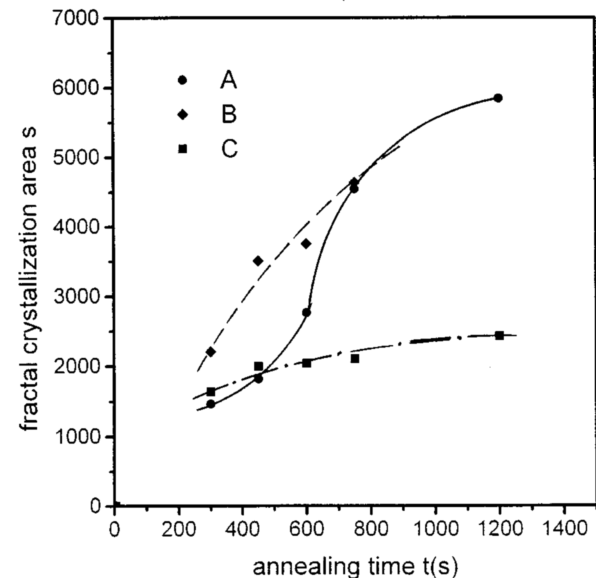

FIG. 5. $S \sim t$ curves of three fractal patterns A, B, and C in Fig. 2 during 130 °C annealing.

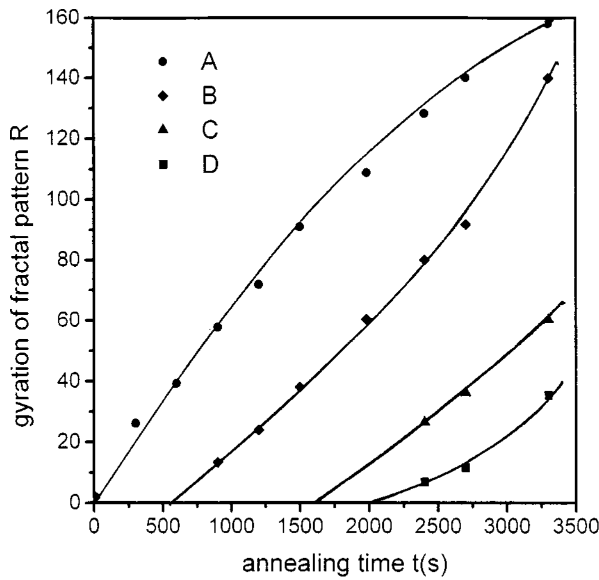

FIG. 6. Relationship between R_g and annealing time t for the fractal patterns *A*, *B*, *C*, and *D* in Fig. 1.

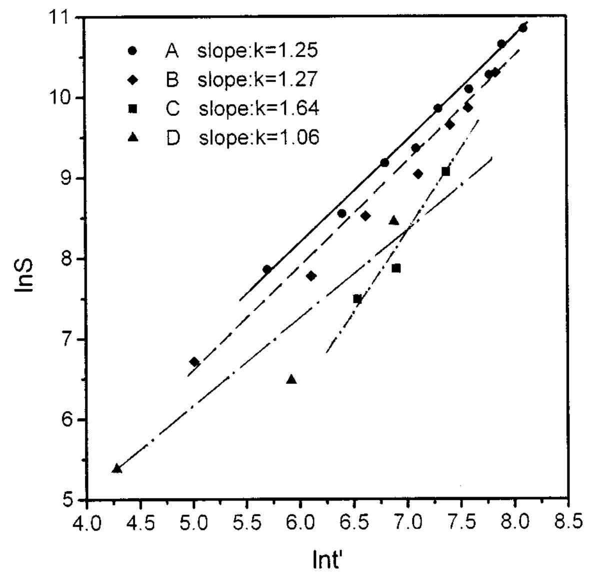

FIG. 8. The k values derived from the slopes of $\ln S$-$\ln t'$ curves for the fractal patterns *A*, *B*, *C*, and *D* in Fig. 1.

DISCUSSIONS

The *in situ* observations and analyses indicate that the fractal crystallization in metal/amorphous semiconductor bilayer films is a complex process. It cannot be simply explained by the DLA model. According to the DLA model, the fractal dimension should keep constant during fractal growth, which is inconsistent with our experimental results. On the other hand, experimental evidence indicates that latent heat released due to crystallization of a-Ge plays an important role in fractal formation. The latent heat can lead to a local temperature rise in the area surrounding the Ge crystallite (the heat of crystallization of amorphous Ge is 1.15×10^4 J/mol[21]). The local temperature rise can stimulate new nuclei to appear randomly in the nearby region, and the processes can be repeated continuously during annealing, resulting in the fractal formation. The process is called the random successive nucleation (RSN) mechanism.[7,8] So RSN process cannot be neglected during fractal formation.

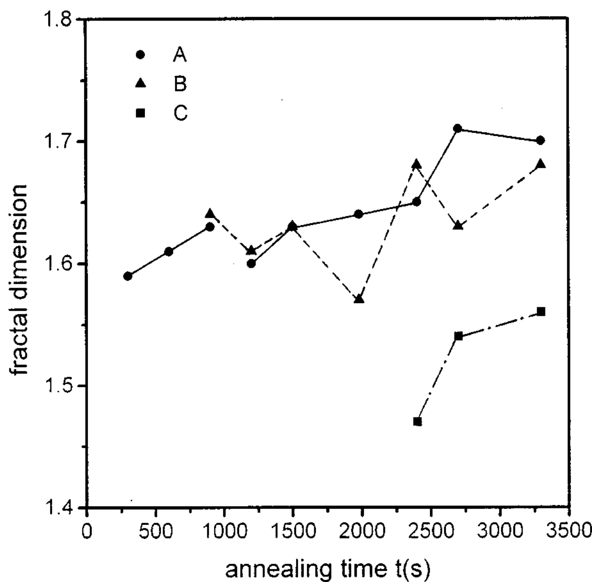

FIG. 7. Fractal dimensions values of the fractal patterns *A*, *B*, and *C* in Fig. 1 during various fractal crystallization stages.

According to the crystallization kinetics, a regular pattern growth in films should obey the power law $S=(t-t_0)^k$, where S is an area of a regular crystallized pattern, t is the annealing time, t_0 is the incubation time, and k is directly related to the growth mechanism ($k=1$ for diffusion-controlled and $k=2$ for reaction-controlled growth in the two-dimensional case).

From the $S\sim t$ and $R_g\sim t$ curves (Figs. 4 and 6) the onset of crystallization can be determined for each fractal pattern in Fig. 1. Hence, k can easily be determined by plotting $\ln S/\ln t'$ ($t'=t-t_0$) as shown in Fig. 8. The k values derived from the slopes are greater than 1 but less than 2 for each fractal pattern. This indicates that fractal growth is in agreement neither with the diffusion-controlled nor with the reaction-controlled mechanism alone. In general, the DLA model belongs to the diffusion-controlled growth, while the RSN model is rather a reaction-controlled mechanism, therefore the kinetics analysis results mean that both diffusion and nucleation play an important role in fractal crystallization.

In Fig. 5, the $S\sim t$ curves of the easily developed fractal pattern *A* (see the $S\sim t$ relationship section) exhibit "∫" shape. It is evident that the k value varies with heating time, i.e., at first k is greater than 1, then close to 1, and finally less than 1. This may represent the whole fractal crystallization process. According to the change of k, the whole process can be divided into three stages: rapid growth, steady growth, and slow growth. At the initial stage, fractal growth was not obstructed by other closely located fractal patterns. Therefore, there existed enough a-Ge so that fractal growth carried on rapidly. With increasing annealing time, fractal patterns became larger, and more and more other patterns approached from the neighborhood, so the growth of pattern *A* was obstructed and became slower. Therefore, the k value decreases gradually. From this point of view, the obstructed and partially obstructed fractals *B* and *C* in Fig. 5 are already on the slow growth stage after 5 min at 130 °C, and the fractals *B*,

C, and *D* in Fig. 4 remain on the first rapid growth stage because of low growth of the fractals at lower temperature.

CONCLUSION

Experimental evidence indicates that fractal growth in Au/*a*-Ge bilayers exhibits three stages: rapid growth, steady growth, and slow growth. At first the growth index k is greater than 1, then close to 1, and finally less than 1. The initial rapid growth stage with $k>1$ indicates both the diffusion and reaction processes play an important role in the fractal crystallization. The decrease of the growth index is caused by the obstruction of the nearby fractals.

*Author to whom correspondence should be addressed. FAX: 86-551-3602803. Electronic address: zhangsy@ustc.edu.cn

[1] F. Oki, Y. Ogawa, and Y. Fujiki, Jpn. J. Appl. Phys. **8**, 1056 (1969).
[2] S. R. Herd, P. Chaudhari, and M. H. Brodsky, J. Non-Cryst. Solids **7**, 309 (1972).
[3] J. R. Bosnell and U. C. Voisey, Thin Solid Films **6**, 161 (1970).
[4] C. C. Tsai, R. J. Nemanich, M. J. Thompson, and B. L. Stafford, J. Vac. Sci. Technol. **21**, 632 (1982).
[5] Z. Tan, S. M. Heard, M. Rapposch, C. E. Bouldin, and J. C. Woicik, Phys. Rev. B **46**, 9505 (1992).
[6] T. J. Konno and R. Sinclair, Philos. Mag. B **66**, 749 (1995).
[7] J. G. Hou and Z. Q. Wu, Phys. Rev. B **40**, 1008 (1989).
[8] B. Q. Li, B. Zheng, S. Y. Zhang, and Z. Q. Wu, Phys. Rev. B **47**, 3638 (1993).
[9] T. A. Witten and L. M. Sander, Phys. Rev. Lett. **47**, 1400 (1981).
[10] Y. Leriah, G. Deutscher, and E. Grubaun, Phys. Rev. A **44**, 8316 (1991).
[11] M. Uwaha and Y. Saito, J. Cryst. Growth **99**, 175 (1990).
[12] R. L. Smith and R. D. Collons, Phys. Rev. A **39**, 5409 (1989).
[13] A. Sugawara, T. Kikukawa, and O. Nittono, Mater. Sci. Eng., A **179/180**, 355 (1994).
[14] B. Bian, T. Ohkubo, and Y. Hirotsu, J. Electron Microsc. **44**, 182 (1995).
[15] B. Bian, T. Tanaka, T. Ohkubo, and Y. Hirotsu, Philos. Mag. A **78**, 157 (1998).
[16] X. Wu, Y. Feng, B. Li, Z. Wu, and S. Zhang, J. Appl. Phys. **75**, 2415 (1994).
[17] R. C. Ball and T. A. Witten, Phys. Rev. A **29**, 2966 (1982).
[18] A. K. Petford-Long, R. C. Doole, C. N. Afonso, and J. Solis, J. Appl. Phys. **77**, 607 (1991).
[19] P. Altuzar and R. Velenzuela, Mater. Lett. **11**, 101 (1991).
[20] Y. Wang, Ph.D. thesis, University of Science and Technology of China (1997).
[21] H. S. Chen and D. Turnbull, J. Appl. Phys. **40**, 4214 (1969).